



OPEN

Solubility of *Ketoconazole* (antifungal drug) in SC-CO₂ for binary and ternary systems: measurements and empirical correlations

Gholamhossein Sodeifian^{1,2,3}✉, Seyed Ali Sajadian^{1,2,4}, Fariba Razmimanesh^{1,2,3} & Seyed Mojtaba Hazaveie^{1,2,3}

One of the main steps in choosing the drug nanoparticle production processes by supercritical carbon dioxide (SC-CO₂) is determining the solubility of the solid solute. For this purpose, the solubility of Ketoconazole (KTZ) in the SC-CO₂ binary system, as well as in the SC-CO₂-menthol (cosolvent), ternary system, was measured at 308–338 K and 12–30 MPa using the static analysis method. The KTZ solubility in the SC-CO₂ ranged between 0.20×10^{-6} and 8.02×10^{-5} , while drug solubility in the SC-CO₂ with cosolvent varied from 1.2×10^{-5} to 1.96×10^{-4} . This difference indicated the significant effect of menthol cosolvent on KTZ solubility in the SC-CO₂. Moreover, KTZ solubilities in the two systems were correlated by several empirical and semiempirical models. Among them, Sodeifian et al., Bian et al., MST, and Bartle et al. models can more accurately correlate experimental data for the binary system than other used models. Also, the Sodeifian and Sajadian model well fitted the solubility data of the ternary system with $AARD\% = 6.45$, $R_{adj} = 0.995$.

Serious fungal infections can increase due to the development of the human immunodeficiency virus (HIV), anti-cancer chemotherapy, and/or the greater utilization of the immuno-suppressive treatments in transplanting the organs¹. Ketoconazole (KTZ) is mainly applied as a synthetic imidazole antifungal drug to treat fungal infections in different forms (oral tablets, topical creams, and gels). It has been applied in immunocompromised patients and advanced prostatic carcinoma^{1,2}. KTZ has very low solubility (17 µg/ml) in the water and higher penetrability; therefore, it has been considered as a class II drug in the biopharmaceutics classification system (BCS). Improving the solubility of pharmaceutical compounds is a challenging subject as it can significantly reduce the oral bioavailability and thus the therapeutic efficacy of drugs².

Reducing particles' size and hence increasing the available surface area can enhance the solubility and bioavailability of pharmaceutical compounds with lower water solubility. Therefore, researchers have applied different processes (such as high-pressure homogenization, evaporation, milling, and sublimation) to reduce particle size in the pharmaceutical industry. Meanwhile, supercritical fluid (SCF) technology has received much attention in medicine to decrease the size of the particles, hence, increasing their dissolution rate and bioactivity. According to studies conducted in this field, the application of supercritical solution methods in particle formation has rapidly expanded. The solubility of drugs in SCFs should be experimentally measured for designing pharmaceutical processes³.

Numerous investigators have demonstrated that solute solubility in the SCFs can be substantially improved with the addition of cosolvents (polar or non-polar)^{4–10}. Gurdial et al.⁴, measured the solubility of o- and m-hydroxy-benzoic acid in acetone-SC-CO₂ and methanol-SC-CO₂ binary mixtures at the temperature range of 318–328 K and the pressure range of 90–200 bar using a continual flow apparatus. Their results indicated that the addition of little amounts of the cosolvents to SC-CO₂ largely enhanced o- and m-hydroxy-benzoic acid

¹Department of Chemical Engineering, Faculty of Engineering, University of Kashan, 87317-53153 Kashan, Iran. ²Laboratory of Supercritical Fluids and Nanotechnology, University of Kashan, 87317-53153 Kashan, Iran. ³Modeling and Simulation Centre, Faculty of Engineering, University of Kashan, 87317-53153 Kashan, Iran. ⁴South Zagros Oil and Gas Production, National Iranian Oil Company, 7135717991 Shiraz, Iran. ✉email: sodeifian@kashanu.ac.ir

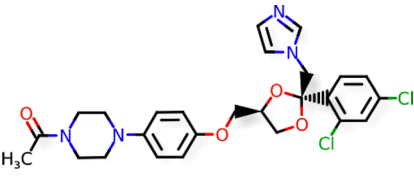
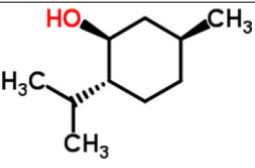
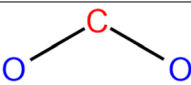
Compound	Formula	Structure	M _w (g/mol)	CAS Number	T _m (K)	λ _{max} (nm)
Ketoconazole	C ₂₆ H ₂₈ Cl ₂ N ₄ O ₄		531	65,277-42-1	423 ± 2	220
L-Menthol	C ₁₀ H ₂₀ O		156.26	2216-51-5	314-317	489
Carbon dioxide	CO ₂		44.01	124-38-9	-	-

Table 1. The utilized solute structure and the respective physico-chemical features (M_w: Molecular weight, T_m: melting point, λ_{max}: λ with maximum absorbance).

solubility. Huang et al.¹¹ evaluated the equilibrium mole fraction of aspirin in SC-CO₂ with and without acetone cosolvent. Their results showed that acetone cosolvent could cause a fivefold increase in aspirin solubility. Also, Koga et al.⁹ investigated influences of cosolvents (octane & ethanol) on the solubility of fatty acids, stearic acid, and stearyl alcohol in SC-CO₂ using a flow-type apparatus and showed the higher effectiveness of ethanol on the solubilities of fatty acids than octane. Hosseini et al.¹² determined the solubility of clozapine and lamotrigine in SC-CO₂ with menthol cosolvent at the temperature range of 313–323 K and the pressure range of 123–337 bar. The applied cosolvent enhanced the solubility of both solutes in SC-CO₂. Consequently, the solubility of numerous compounds has been experimentally determined in the SCFs^{13–20}. However, the measurement of the solubility of drugs in the SCFs under diverse pressure and temperature conditions is costly and laborious²¹. In this regard, thermodynamic models have been developed to decrease the number of required experimental measurements. Compared to the other SCFs, SC-CO₂ has been widely employed in SCF processes due to its special thermodynamic and heat transfer properties. Additionally, CO₂ is non-toxic, non-flammable, cost-effective, abundant at high levels of purity, and environmentally-friendly with comparatively lower critical pressures and temperatures (7.38 MPa & 304.1 K)^{22–27}. Several models have been applied to correlate and predict solids solubility at supercritical conditions, among which empirical and semiempirical methods^{28–34}, equations of state (EoS) (including cubic and non-cubic models)^{35–43}, expanded liquid model⁴⁴, intelligent computational techniques (e.g. artificial neural networks (ANN) and least square support vector machine (LS-SVM) networks), and combination of grey wolf optimizer and support vector machines (GWO-SVM) networks^{27,45} can be mentioned. Some characteristics such as acentric factor, and molar volume, as well as the solid vapor pressures, are essential for the calculations of EoS based models. These parameters are, however, unavailable and thus must be estimated by the group contribution techniques leading to attenuated accuracy. To overcome this drawback, several researchers have applied different empirical and semiempirical models to correlate the solubility data^{46–57}.

In this study, a static analysis procedure was employed to determine the solubility of KTZ in SC-CO₂ at different temperature and pressure conditions with and without cosolvent. The solubility of KTZ in the SC-CO₂ with cosolvent has not been experimentally measured so far. Moreover, drug solubility in the SC-CO₂ (i.e., the binary system) was correlated by ten semi-empirical models, including Chrastil²⁸, Sparks et al.³⁴, Bian et al.⁴¹, Bartle et al.⁵¹, MST³², Kumar-Johnston²⁹, Jouyban et al.³³, as well as Sodeifian et al.¹⁴, models. Also, MST³², González et al.⁵², Soltani-Mazloumi⁴⁹, and Sodeifian-Sajadian⁵⁸ models were applied to fit the solubility data of KTZ in the ternary system. Finally, the ability of different models was investigated in terms of three statistical measures: AARD, %, and R_{adj}.

Experimental

Materials. In this work, Fadak Company (Kashan: Iran) provided carbon dioxide (CAS Number 124-38-9) with the purity of 99.99%. KTZ with the purity of 99% (CAS Number 65277-42-1) was provided by Arasto Pharmaceutical Company (Tehran, Iran). The above materials were applied with no additional treatment. Also, menthol with the purity (Ph Eur) of 99.0% (CAS Number 2216-51-5) and methanol (GC) at the purity level of 99% (CAS Number 67-56-1) were purchased from Merck (German). Tables 1 presents the structures and physicochemical features of KTZ.

Experimental apparatus. Figure 1 shows the laboratory setup used for determining solubility data of KTZ in SC-CO₂ with/without cosolvent (static method). The experimental setup was completely explained in our previous paper⁵⁸. It includes a carbon dioxide tank, filter, refrigerator unit, reciprocating pump equipped with air compressor for supplying driving force, solubility cells, pressure gauge, digital pressure transmitter, digital ther-

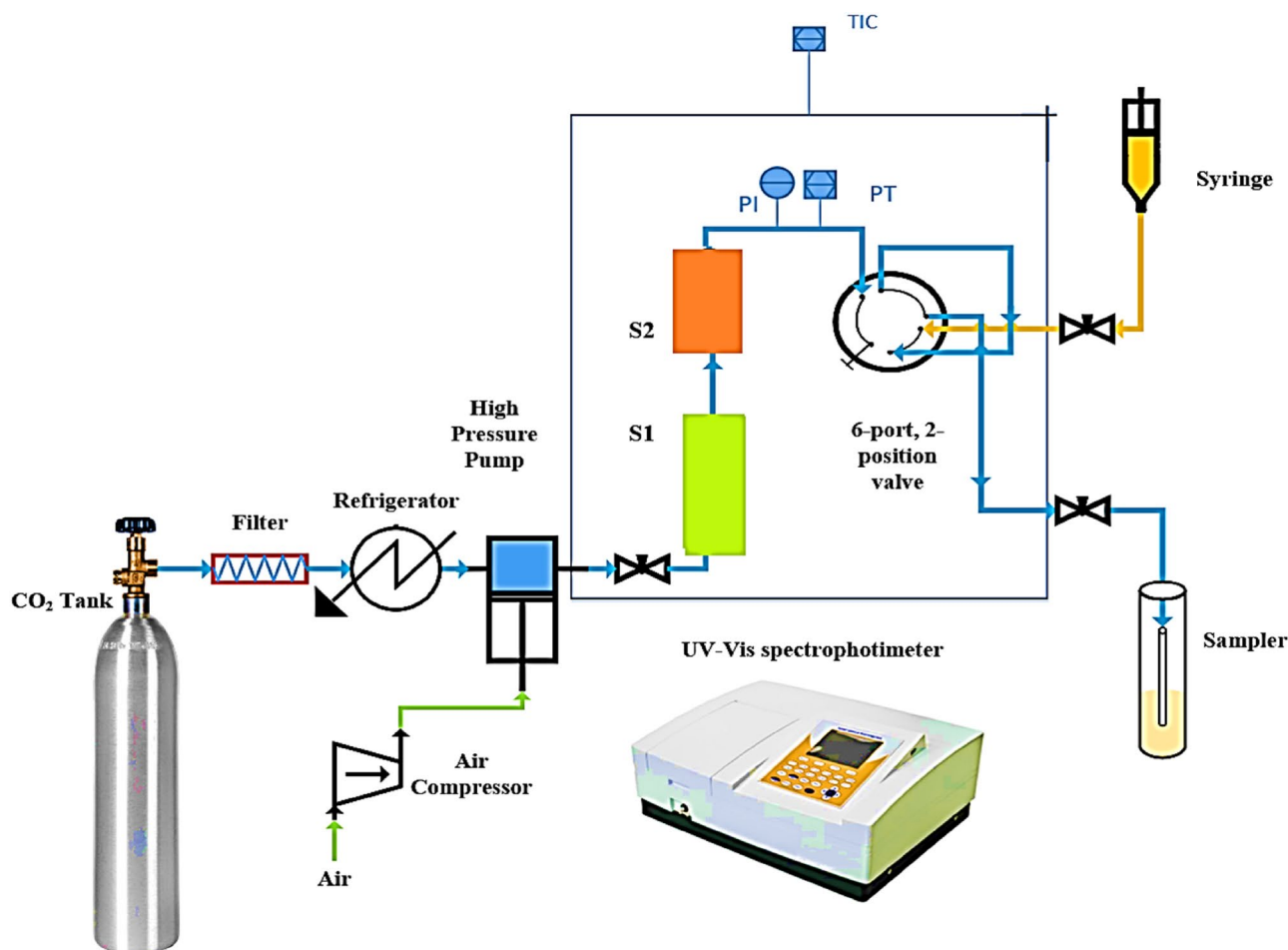


Figure 1. A schema of the utilized setup to measure solubility.

meter, oven, microliter valve, sample collector, flow meter, 1/8" piping, and connections. Pressure quantities were recorded at the accuracy of ± 0.1 MPa using both the pressure gauge (WIKA, Germany, Code EN 837-1) and pressure transmitter. To maintain the experimental temperature, the equilibrium cell was located in a precise oven (Froilabo Model, AE-60, France), which could retain the temperature within ± 0.1 K.

The amount of menthol and drug in saturator cell 1 (S1) and saturator cell 2 (S2) were 5 and 2 g, respectively. A magnetic stirrer (100 rpm) was applied to accelerate the equilibration and improve saturation of the particles in cells. The sintered filter was put on the top of the column to prevent the escape of menthol particles (as either powder or liquid droplets). In this research, the equilibrium time was considered 60 min (as determined by preliminary experiments). At the end of static time, $600 \pm 0.6\%$ μL of the saturated SC-CO₂ was depressurized into the collection vial containing 5 ml methanol. Eventually, the loop was washed with the solvent collected in the collection vial, and the final volume of the solution was adjusted to $5 \text{ mL} \pm 0.6\%$. It should be noted that the experiments were carried out in triplicates. Consequently, the solubility of KTZ was determined by measuring the absorbance at λ_{max} , 220 nm (at which menthol wavelength is transparent) on the UNICO-4802 UV-Vis spectro-photometer with 1-cm pass length quartz cells. Finally, the calibration curve (with regression coefficient 0.996) was applied to obtain the medicine concentrations in the collection vial.

As presented in Tables 2 and 3, solubilities of KTZ (in the equilibrium mole fraction of the solute (y) and the grams of solute (S) per liter of SC-CO₂ with/without cosolvent) were evaluated at the pressure range of 12–30 MPa and temperature range of 308–338 K. Finally, Span–Wagner equation was used to obtain the CO₂ density⁵⁹.

Results and discussion

Binary system. In our previous study, the reliability of the solubility setup was evaluated by determining the solubility of naphthalene and alpha-tocopherol in SC-CO₂ at different pressures and temperatures and comparing them with the corresponding data in the literature⁶⁰. In general, the authors systematically check and calibrate the device before testing naphthalene and alpha-tocopherol solubilities in SC-CO₂.

It should be mentioned that the mole fraction and solubility (S(g/L)) of KTZ in SC-CO₂ were measured at different temperature and pressure conditions (Table 2). Each experimental data was measured in triplicate to enhance the data reliability. The relative standard uncertainty of the solubility data was below 0.05. The relative standard uncertainty (U_r) can be calculated by the following equation:

Temperature ^a (K)	Pressure ^a (MPa)	Density ^b (kg/m ³)	Binary			
			$y_2 \times 10^5$ (Mole Fraction)	Standard deviation of the mean, $SD(\bar{y}) \times (10^5)$	Expanded uncertainty of mole fraction ($10^5 U$)	S (Solubility (g/l))
308	12	768.42	0.17	0.001	0.008	0.016
	15	816.06	0.34	0.003	0.016	0.034
	18	848.87	0.44	0.017	0.039	0.045
	21	874.4	0.62	0.017	0.044	0.066
	24	895.54	0.80	0.034	0.077	0.087
	27	913.69	0.94	0.017	0.054	0.104
	30	929.68	1.09	0.051	0.114	0.122
318	12	659.73	0.07	0.003	0.007	0.006
	15	743.17	0.32	0.010	0.027	0.036
	18	790.18	0.85	0.034	0.079	0.081
	21	823.7	1.31	0.035	0.090	0.130
	24	850.1	1.68	0.069	0.157	0.173
	27	872.04	2.11	0.035	0.115	0.222
	30	890.92	2.59	0.086	0.207	0.279
328	12	506.85	0.04	0.001	0.003	0.003
	15	654.94	0.30	0.002	0.015	0.026
	18	724.13	0.98	0.035	0.082	0.086
	21	768.74	1.82	0.052	0.131	0.169
	24	801.92	2.76	0.050	0.160	0.267
	27	828.51	4.02	0.087	0.247	0.402
	30	850.83	4.81	0.068	0.252	0.494
338	12	384.17	0.02	0.0006	0.001	0.001
	15	555.23	0.22	0.010	0.023	0.015
	18	651.18	0.90	0.017	0.056	0.077
	21	709.69	2.29	0.052	0.145	0.196
	24	751.17	4.2	0.032	0.198	0.381
	27	783.29	6.02	0.085	0.316	0.569
	30	809.58	8.02	0.121	0.427	0.784

Table 2. The experimental data of KTZ solubility in SC-CO₂ based on distinct conditions (The experimental standard deviation and the experimental standard deviation of the mean (SD) were obtained by

$S(y_k) = \sqrt{\frac{\sum_{j=1}^n (y_j - \bar{y})^2}{n-1}}$ and $SD(\bar{y}) = \frac{S(y_k)}{\sqrt{n}}$ respectively. n is the number of times each experimental data was measured ($n = 3$, in this work). Expanded uncertainty is $U = k^* u_{combined}$ and the relative combined standard uncertainty is defined as $u_{combined} / y = \sqrt{\sum_{i=1}^N (P_i u(x_i)/x_i)^2}$ in which $u(x_i)/x_i$ is the relative standard uncertainty of each input estimate (x_i) and P_i is known positive or negative number having negligible uncertainties. y_2 and S are mole fraction of solute in binary system and solubility of solute in SC-CO₂, respectively. ^aStandard uncertainty u are $u(T) = 0.1$ K; $u(p) = 1$ bar. Also, the relative standard uncertainties are obtained below 0.05 for mole fractions and solubilities. The value of the coverage factor $k = 2$ was chosen on the basis of the level of confidence of approximately 95 percent. ^bData from the Span–Wagner equation of state⁶².

$$U_s = \frac{S(y_k)}{\bar{y}} \quad (1)$$

$$S(y_k) = \sqrt{\frac{\sum_{j=1}^n (y_j - \bar{y})^2}{n-1}} \quad (2)$$

where $S(y_k)$ and n are the experimental standard deviation and the number of measurements of each experimental data ($n = 3$, in this work), respectively.

y and S (g/L) values respectively ranged between 0.20×10^{-6} and 8.02×10^{-4} , and 0.001 and 0.784. Finally, the greatest and least values of KTZ solubility were observed at (338 K, 30 MPa) and (338 K, 12 MPa), respectively.

Figure 2a shows an increase in the solubility of KTZ with pressure increment at each isotherm. An enhancement in the density also increased the solubility at the elevated pressures. Generally, SC-CO₂ density and solute vapor pressure are the two key factors contributing to the solubility of the solute in SC-CO₂. The solubility showed

Temperature ^a (K)	Pressure ^a (MPa)	Menthol	Ternary	Standard deviation of the mean, SD (y') $\times 10^4$	Expanded uncertainty of mole fraction (10^4 U)	E (cosolvent effect)
		$y_3 \times 10^3$	$y'_2 \times 10^4$ (Mole Fraction)			
308	12	16.40	0.27	0.003	0.014	16.1
	15	17.32	0.38	0.001	0.017	9.7
	18	18.69	0.43	0.003	0.020	9.4
	21	19.43	0.46	0.005	0.022	9.7
	24	20.43	0.54	0.003	0.024	6.8
	27	22.17	0.59	0.002	0.026	5.3
	30	23.63	0.62	0.008	0.032	4.9
318	12	14.70	0.21	0.001	0.010	30.6
	15	16.32	0.39	0.003	0.019	12.3
	18	17.34	0.53	0.008	0.029	11.1
	21	19.42	0.69	0.003	0.031	7.7
	24	21.09	0.87	0.003	0.039	5.2
	27	24.34	1.02	0.007	0.047	4.0
	30	26.36	1.11	0.009	0.051	3.3
328	12	12.36	0.18	0.005	0.013	45.9
	15	15.84	0.41	0.006	0.023	16.6
	18	18.45	0.63	0.005	0.030	11.5
	21	19.94	0.90	0.008	0.043	5.9
	24	22.34	1.12	0.004	0.050	3.9
	27	26.34	1.31	0.009	0.060	3.5
	30	29.70	1.65	0.017	0.080	2.9
338	12	12.09	0.12	0.003	0.008	61.2
	15	16.12	0.45	0.001	0.020	34.4
	18	19.18	0.76	0.003	0.034	11.6
	21	25.33	1.01	0.015	0.054	5.5
	24	24.59	1.34	0.020	0.072	3.7
	27	30.82	1.70	0.017	0.082	2.8
	30	32.87	1.96	0.025	0.100	2.4

Table 3. The experimental data of KTZ solubility in SC-CO₂ – menthol based on distinct conditions. y_3 , y'_2 and e are mole fraction of menthol, mole fraction of solute in ternary system and cosolvent effect, respectively. The experimental standard deviation of the mean (SD) were obtained by $SD(\bar{y}) = \frac{S(y_k)}{\sqrt{n}}$. n is the number of times each experimental data was measured ($n=3$, in this work). Expanded uncertainty is $U = k^* u_{combined}$ and the relative combined standard uncertainty is defined as $u_{combined} / y = \sqrt{\sum_{i=1}^N (P_i u(x_i)/x_i)^2}$ in which $u(x_i)/x_i$ is the relative standard uncertainty of each input estimate (x_i) and P_i is known positive or negative number having negligible uncertainties. ^aStandard uncertainty u are $u(T) = 0.1$ K; $u(p) = 1$ bar. Also, the relative standard uncertainties are obtained below 0.05 for mole fractions and solubilities. The value of the coverage factor $k=2$ was chosen on the basis of the level of confidence of approximately 95 percent. ^bData from the Span–Wagner equation of state⁶².

an ascending trend with increasing density and solute vapor pressure. At pressures below the crossover region, where the influence of increased solvent density on the solute solubility dominates over decreased solute vapor pressure, the solid solute exhibited higher solubility at lower temperatures rather than higher ones. At the top of the crossover region, when temperature increased, the solubility incremented more rapidly with pressure enhancement, which might be due to the competing effects of the reduction of SC-CO₂ density and the increase of solute vapor pressure.

Figure 2a presents a pressure range of 19–20 MPa that was considered as the crossover pressure area for KTZ in the binary system. In general, several studies demonstrated that the solute vapor pressure and SC-CO₂ density are the major parameters below and top of the crossover area^{26,60–63}. Yamini and Moradi¹ measured KTZ solubility in SC-CO₂ at 12.2–35.5 MPa and 308–348 K considering the absorbance at λ_{max} (220 nm). In the present work, the mole fraction of KTZ dissolved in SC-CO₂ (in pressure and temperature spans of 12–30 MPa and 308–338 K) was 0.20×10^{-6} and 8.02×10^{-5} . Their solubility data at this condition ranged from 0.7×10^{-6} to 8.16×10^{-5} . The mean standard deviation between their experimental data and the present work was 2%. The effects of temperature and pressure on the solubility were the same for both works.

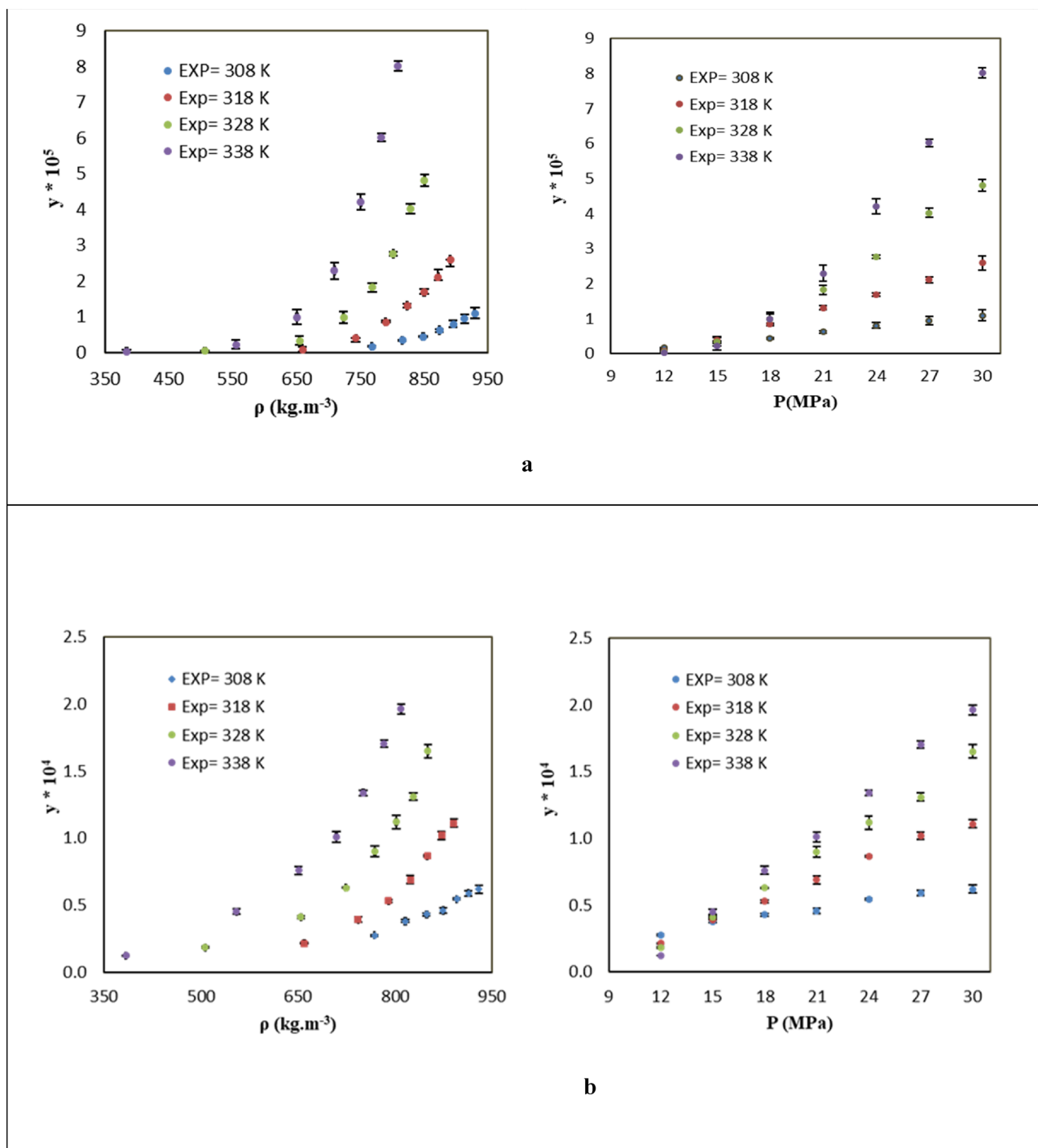


Figure 2. The KTZ solubility in (a) binary system and (b) ternary system.

Ternary systems. Figure 2b and Table 3 report KTZ solubility in SC-CO₂ with cosolvent (menthol) under different pressures and temperatures. Accordingly, solubility based on the solute mole fraction (y) ranged from 1.2×10^{-5} to 1.96×10^{-4} . Each experimental data was measured three times to enhance the reliability of the solubility data. Figure 2b presents an increase in KTZ solubility with the pressure increment at all isotherms. The increase of density with rising the pressure led to the more powerful solvation ability of SC-CO₂ and thus enhanced the solid solubility. The largest increment in solubility with rising pressure was observed at the highest temperature, which can be assigned to the impacts of the temperatures and pressures on the solvent density and pressure of the solute vapor¹⁰. As stated previously, temperature influences the solvating power by two challenging factors: the solvent density and pressure of the solute vapor. Therefore, an increment in temperature will decrease the solubility below the crossover pressure area and also increased the solubility above the crossover pressure area. Finally, the crossover point in the ternary system was between 13 and 15 MPa.

Model	Formula
Chrastil ²⁸	$c = \rho^{a_0} \exp(\frac{a_1}{T} + a_2)$
K-J ²⁹	$\ln(y_2) = a_0 + a_1 \rho + \frac{a_2}{T}$
Bartle et al. ⁵¹	$\ln(\frac{y_2 P}{P_{ref}}) = a_0 + \frac{a_1}{T} + a_2(\rho - \rho_{ref})$
MST ³²	$T \ln(y_2 P) = a_0 + a_1 \rho + a_2 T$
Sparks et al. ⁴²	$c_2^* = \rho_{r,1}^{a_0+a_1} \rho_{r,1} \exp(a_2 + \frac{a_3}{T})$
Bian et al. ⁴¹	$y_2 = \rho^{(a_0+a_1\rho)} \exp(\frac{a_2}{T} + \frac{a_3\rho}{T} + a_4)$
Jouyban et al. ³³	$\ln y_2 = a_0 + a_1 \rho + a_2 P^2 + a_3 P T + \frac{a_4 T}{P} + a_5 \ln(\rho)$
Sodeifian et al. ¹⁴	$\ln y_2 = a_0 + a_1 \frac{P^2}{T} + a_2 \ln(\rho T) + a_3(\rho \ln \rho) + a_4 P \ln T + a_5 \frac{\ln \rho}{T}$

Table 4. A brief statement of the density-based models utilized in the present research (c , ρ , T , P , P_{ref} , ρ_{ref} , y_2 and a_0 – a_5 are solubility of solute, density of SC-CO₂, temperature, pressure, reference pressure, reference density, mole fraction in binary system and adjustable parameters, respectively).

In the ternary system (solute-SC-CO₂-cosolvent), the enhancement factor has been considered to study the cosolvent effect. This factor is the ratio of the obtained solubility of solute within the ternary system to that of the binary system. By investigating the presented results in Table 3, it can be founded out that the solubility was increased by adding menthol to SC-CO₂. The cosolvent effect “ e ” was applied to better evaluate the solubility enhancement^{7,64}.

$$e = \frac{y_2'(P, T, y_3)}{y_2(P, T)} \quad (3)$$

Table 3 presents the values of “ e ” in this study. The highest cosolvent effect was (61.2-fold) is related to the pressure of 12 MPa and a temperature of 338 K. Other researchers also reported the cosolvent effect in their studies. Hosseini et al.¹², compared the solubility of clozapine and lamotrigine in SC-CO₂ (with solid cosolvent (menthol)) with the cosolvent-free condition. The solubility of clozapine showed an approximate 56-fold enhancement while that of lamotrigine was increased almost 8 times. Sabet et al.⁶⁵ measured acetaminophen solubility in SC-CO₂ with and without menthol solid cosolvent under different temperatures and pressures. As shown by the results, menthol strongly augmented acetaminophen solubility by (8.27-fold). Gupta and Thakur⁶⁶ investigated the solubility of phenytoin in SC-CO₂. They concluded that solid solute solubility in SC-CO₂ is only 3 $\mu\text{mol/mol}$ while its solubility increased to 1302 $\mu\text{mol/mol}$ (at 45 °C and at 196 bar) in SC-CO₂ with menthol solid cosolvent. Notably, interactions between menthol and phenytoin resulted in a 400-fold solubility enhancement. Sodeifian and Sajadian¹⁰ determined the solubility of letrozole under different circumstances in SC-CO₂ with and without menthol. Solid co-solvent could increase letrozole solubility up to 7.1 folds compared to the binary system (without solid cosolvent).

In general, the increase in the solubility of solids in ternary systems (CO₂ + cosolvent) can be attributed to the increase in solvent density, dipole–dipole interactions, and also hydrogen bonding between the solute and the cosolvent⁶⁷. In this case, upon adding menthol to the cell, the density of the SCF enhanced, leading to an increment in the solubility. The polarity of SC-CO₂ can also be affected by the cosolvent. Menthol enhanced the solubility of KTZ in CO₂ due to the presence of a hydroxyl (polar) group and a hydrocarbon group (nonpolar) in the respective structures. As a result, it can be concluded that stronger attractive polar interaction and hydrogen bonding could lead to greater solubility. Also, by comparing values of e in Table 3, it can be inferred that cosolvent effects decreased with the increment of the pressure, which is compatible with the published studies^{4–6,11}.

Correlation of the binary system. The present study considered ten semiempirical equations for correlating KTZ solubility in SC-CO₂, as listed in Table 4. Figure 3 depicts the outputs of the correlation at different temperatures. Then, statistical criteria were employed to investigate the abilities of semiempirical models. As a general rule, the more adjustable parameters lead to more accurate correlations. To provide a reliable accuracy criterion to compare the models with different numbers of adjustable parameters, AARD and R_{adj} with the following equations were used⁶⁸:

$$AARD, \% = \frac{100}{N_i - Z} \sum_{i=1}^{N_i} \frac{|y_2^{calc} - y_2^{exp}|}{y_2^{exp}} \quad (4)$$

So that Z represents the number of the adjustable variables for each model.

$$R_{adj} = \sqrt{|R^2 - (Q(1 - R^2)/(N - Q - 1))|} \quad (5)$$

where N refers to the numbers of data points in each set. Moreover, Q stands for the numbers of the independent variables in each equation. R_{adj} can be used to compare models with different numbers of independent variables and R^2 represents the correlation coefficient⁶⁹.

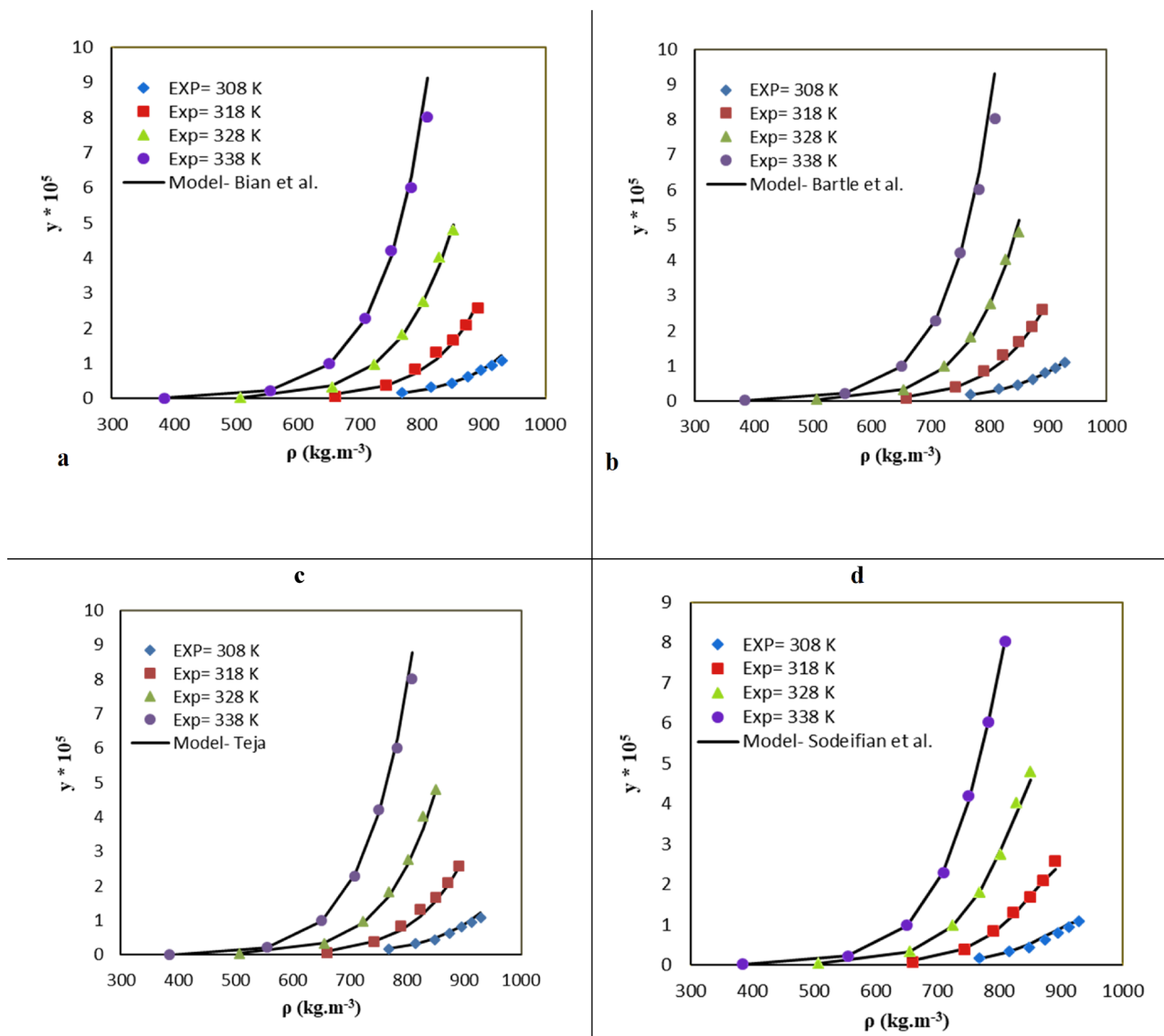


Figure 3. The experimental (points) and computed (line) solubility of KTZ (binary system) by (a) Bian et al., (b) Bartle et al. (c) MST & (d) Sodeifian et al., models.

$$R^2 = 1 - \frac{SS_E}{SS_T} \quad (6)$$

$$SS_T = \sum (y_{\text{exp}})^2 - \frac{(\sum y_{\text{exp}})^2}{N} \quad (7)$$

$$SS_E = \sum (y_{\text{exp}} - y_{\text{model}})^2 \quad (8)$$

where SS_E is the error of the sum of squares and SS_T is the total sum of squares.

Correlation results and optimal values of the parameters are presented in Table 5. The mean-values of AARD% for Chrastil, Sparks et al., K-J, Bian et al., Bartle et al., MST, Jouyban et al., and Sodeifian et al., models were 10.01, 11.52, 09.93, 09.22, 07.55, 09.61, 15.11 and 06.94%, respectively. According to the ANOVA results, it can be concluded that Bian et al., ($R_{\text{adj}} = 0.991$), MST ($R_{\text{adj}} = 0.996$), and Sodeifian et al., ($R_{\text{adj}} = 0.999$) models could more accurately correlate KTZ solubility (Fig. 3).

The energy term describing the temperature term coefficient in Chrastil, Sparks et al., and Bartle et al., models were considered to determine the heat of solvation (ΔH_{sol}), the vaporization heat of the solute (ΔH_{vap}), and total heat (ΔH_t). The second tunable variables of Chrastil, Sparks et al., and Bartle et al., models were used to calculate ΔH_t and ΔH_{vap} , respectively. Also, ΔH_{sol} was calculated based on the difference between ΔH_{vap} and ΔH_{total} . Based on Table 6, the enthalpy of KTZ dissolution in SC-CO₂ and ΔH_{total} were 99.32 and 101.70 kJ.mol⁻¹, respectively. Also, ΔH_{vap} was calculated by Bartle et al., as 121.80 kJ.mol⁻¹. According to our data, solvation and

Model	a_0	a_1	a_2	a_3	a_4	a_5	AARD%	R_{adj}
Chrastil	11.107	-11,945.812	-39.215	-	-	-	10.01	0.990
Sparks et al.,	5.9141	2.3629	25.666	-41.5872	-	-	11.52	0.989
K-J	16.75	0.0144	-1273.9	-	-	-	09.93	0.985
Bian et al.,	-4.0301	0.0020	-10,553.88	-2.2336	-10.6230	-	09.22	0.991
Bartle et al.,	37.82	-14,650.1	0.0175	-	-	-	07.55	0.989
MST	-18,858.47	245,948.22	38.761	-	-	-	09.61	0.996
Jouyban et al.,	-56.512	-53.3345	-0.00002	0.00007	-1.5936	37.1537	15.11	0.989
Sodeifian et al.,	-25.7435	-0.503	3.2028	0.0027	0.003600	-1910.229	06.94	0.999

Table 5. The correlation results of the KTZ – CO₂ system provided by semi-empirical models (AARD, R_{adj} and a_0 - a_5 are average absolute relative deviation, adjusted correlation coefficient and adjustable parameters, respectively).

Compound	ΔH_{total} (kJ mol ⁻¹)	ΔH_{vap} (kJ mol ⁻¹) ^b	ΔH_{sol} (kJ mol ⁻¹) ^d
Ketoconazole	99.32 ^a	121.80	-22.48
	105.09 ^c	121.80	-16.71

Table 6. The vaporization (ΔH_{vap}), approximated total (ΔH_{total}), and solvation (ΔH_{sol}) enthalpy for KTZ. ^aObtained from the Chrastil's model. ^bObtained from the Bartle et al., model. ^cObtained from the Sparks et al., model. ^dObtained from the difference between the ΔH_{vap} and ΔH_{total} .

Model	Formula
MST ⁵³	$T \ln \left(\frac{y_2' P}{P_{ref}} \right) = a_0 + a_1 \rho_1 + a_2 T + a_3 y_3$
Sodeifian-Sajadian ⁵⁸	$\ln \left(y_2' \right) = (a_0 + \frac{a_1 \rho_1}{T}) \ln(\rho_1) + a_2 \rho_1 + a_3 \ln(y_3 P)$
González et al. ⁵²	$\ln \left(y_2' \right) = a_0 \ln(\rho_1) + a_1 \ln(y_3) + \frac{a_2}{T} + a_3$
Soltani-Mazloumi ⁴⁹	$\ln \left(y_2' \right) = a_0 + \frac{a_1}{T} + \frac{a_2}{T} \rho_1 - a_3 \ln(P) + a_4 \ln(y_3 \rho_1 T)$

Table 7. A brief statement of the density-based models utilized in the present research (ρ_1 , T , P , P_{ref} , y_2' , y_3 and a_0 - a_6 are density of SC-CO₂, temperature, pressure, reference pressure, mole fraction in ternary system, mole fraction of cosolvent and adjustable parameters, respectively).

vaporization processes are endothermic and exothermic, respectively. The value of ΔH_{vap} was bigger than ΔH_{total} . Due to differences between ΔH_{total} and ΔH_{vap} values, ΔH_{sol} values from different models were calculated -22.48 and -20.10 kJ.mol⁻¹.

Correlation of the ternary system. The present research assessed the correlation of KTZ solubilities in SC-CO₂ with menthol by five semiempirical models (Table 7). Menthol solubility in SC-CO₂ was reported in previous work⁵⁸. The statistical criteria (*i.e.*, R_{adj} and AARD%) were applied to examine the capability of the presented models. A genetic algorithm was also used to obtain adjustable parameters. Figure 4 and Table 8 present the compatibility of KTZ solubility data with the semiempirical results. The highest accuracy was offered by the Sodeifian and Sajadian model (AARD,% = 06.45, R_{adj} = 0.995), followed by those of González et al. (AARD,% = 07.51, R_{adj} = 0.991), MST (AARD,% = 08.97, R_{adj} = 0.986) and Soltani and Mazloumi (AARD,% = 07.09, R_{adj} = 0.992), respectively.

Conclusions

In this research, the KTZ solubility in SC-CO₂ (with and without menthol) was experimentally measured at the temperature range of 308–338 K and the pressure range of 12–30 MPa using spectrophotometric analysis. The tests were carried out in triplicates to enhance the reliability of the solubility data. Moreover, the mole fractions (y) and KTZ solubility (S (g/L)) in SC-CO₂ (binary system) ranged between 0.001 and 0.784 and 0.2×10^{-6} and 8.02×10^{-5} , while the mole fractions of the drug in the SC-CO₂ with cosolvent (*i.e.*, the ternary system) ranged in 1.2×10^{-5} – 1.96×10^{-4} . Therefore, it can be concluded that the solubility increased in the presence of menthol. Several semi-empirical and empirical models were utilized for correlating experimental results of binary and ternary systems. Among them, Sodeifian et al. model managed to correlate the experimental data for the mentioned binary system at higher accuracy. In the case of the ternary system, the highest accuracy was provided by the Sodeifian and Sajadian model.

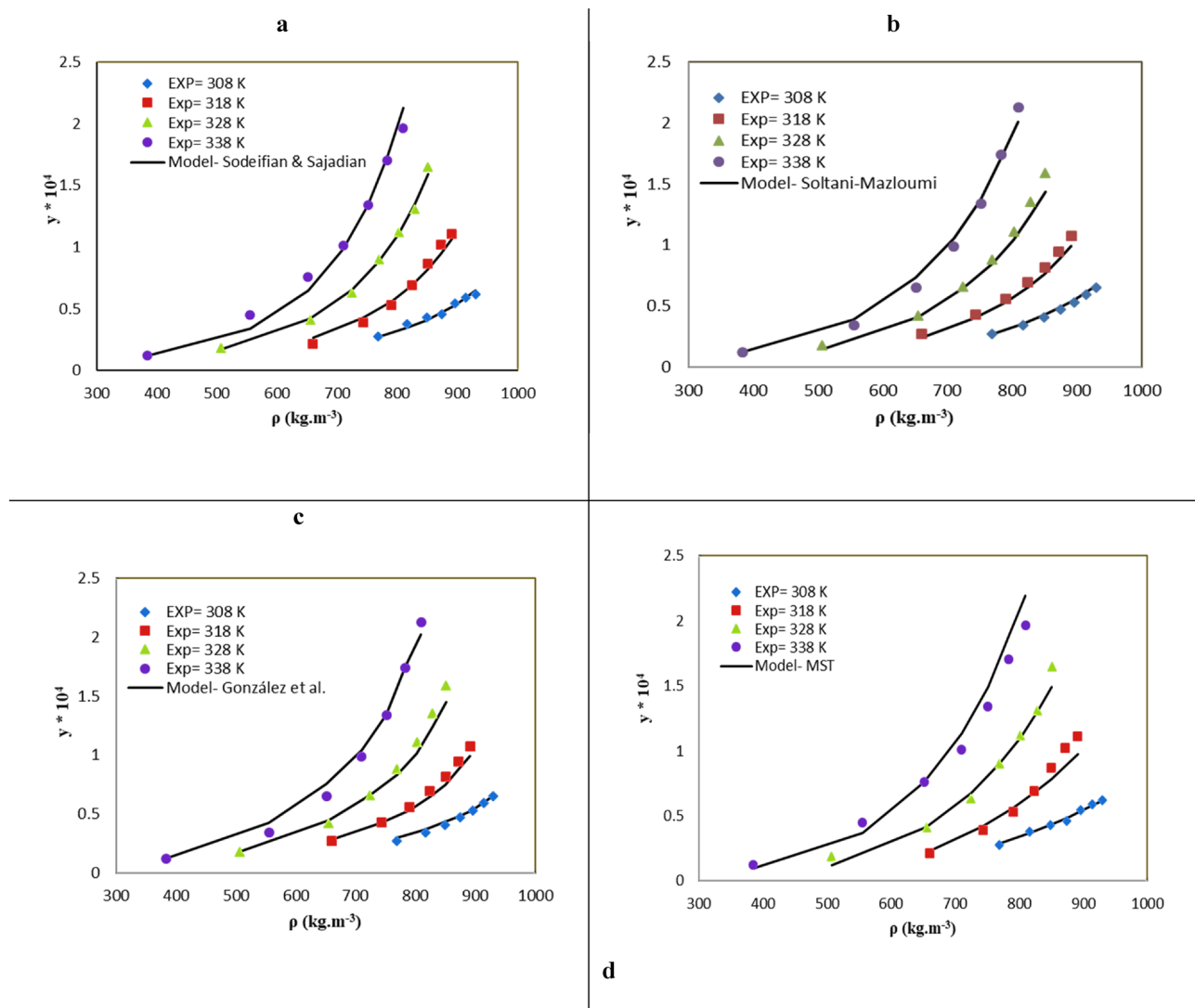


Figure 4. The experimental (points) and calculated (line) of KTZ solubility (ternary system) by (a) Sodeifian and Sajadian, (b) Soltani-Mazloumi, (c) González et al., and (d) MST models.

Model	a_0	a_1	a_2	a_3	a_4	AARD%	R_{adj}
MST	-10,884.4360	3.1002	21.7610	28.803	-	8.97	0.986
González et al.,	2.902	0.657	-4544.27	-12.26	-	7.51	0.991
Sodeifian—Sajadian	-2.852	-1.0502	0.0339	0.153	-	6.45	0.995
Soltani-Mazloumi	10.489	-8213.5	2.155	0.4203	0.2776	7.09	0.992

Table 8. The correlation results of the KTZ–Menthol–CO₂ system provided by the semi empirical models (AARD, R_{adj} and a_0 – a_6 are average absolute relative deviation, adjusted correlation coefficient and adjustable parameters, respectively).

Received: 3 January 2021; Accepted: 25 March 2021
Published online: 06 April 2021

References

1. Yamini, Y. & Moradi, M. Measurement and correlation of antifungal drugs solubility in pure supercritical CO₂ using semiempirical models. *J. Chem. Thermodyn.* **43**, 1091–1096. <https://doi.org/10.1016/j.jct.2011.02.020> (2011).
2. Maniruzzaman, M. *et al.* Development and optimization of ketoconazole oral strips by means of continuous hot-melt extrusion processing. *J. Pharm. Pharmacol.* **68**, 890–900. <https://doi.org/10.1111/jph.12569> (2016).

3. Manna, L. & Banchero, M. Solubility of tolbutamide and chlorpropamide in supercritical carbon dioxide. *J. Chem. Eng. Data* **63**, 1745–1751. <https://doi.org/10.1021/acs.jced.8b00050> (2018).
4. Foster, N. R., Singh, H., Yun, S. J., Tomasko, D. L. & Macnaughton, S. J. Polar and nonpolar cosolvent effects on the solubility of cholesterol in supercritical fluids. *Ind. Eng. Chem. Res.* **32**, 2849–2853. <https://doi.org/10.1021/ie00023a056> (1993).
5. Ekart, M. P. *et al.* Cosolvent interactions in supercritical fluid solutions. *AIChE J.* **39**, 235–248. <https://doi.org/10.1002/aic.690390206> (1993).
6. Ting, S. S., Tomasko, D. L., Foster, N. R. & Macnaughton, S. J. Solubility of naproxen in supercritical carbon dioxide with and without cosolvents. *Ind. Eng. Chem. Res.* **32**, 1471–1481. <https://doi.org/10.1021/ie00019a022> (1993).
7. Huang, Z., Kawi, S. & Chiew, Y. Solubility of cholesterol and its esters in supercritical carbon dioxide with and without cosolvents. *J. Supercrit. Fluids* **30**, 25–39. [https://doi.org/10.1016/S0896-8446\(03\)00116-5](https://doi.org/10.1016/S0896-8446(03)00116-5) (2004).
8. Reddy, S. N. & Madras, G. Modeling of ternary solubilities of solids in supercritical carbon dioxide in the presence of cosolvents or cosolutes. *J. Supercrit. Fluids* **63**, 105–114. <https://doi.org/10.1016/j.supflu.2011.11.016> (2012).
9. Koga, Y., Iwai, Y., Hata, Y., Yamamoto, M. & Arai, Y. Influence of cosolvent on solubilities of fatty acids and higher alcohols in supercritical carbon dioxide. *Fluid Phase Equilib.* **125**, 115–128. [https://doi.org/10.1016/S0378-3812\(96\)03090-7](https://doi.org/10.1016/S0378-3812(96)03090-7) (1996).
10. Sodeifian, G. & Sajadian, S. A. Solubility measurement and preparation of nanoparticles of an anticancer drug (Letrozole) using rapid expansion of supercritical solutions with solid cosolvent (RESS-SC). *J. Supercrit. Fluids* **133**, 239–252. <https://doi.org/10.1016/j.supflu.2017.10.015> (2018).
11. Huang, Z., Lu, W. D., Kawi, S. & Chiew, Y. C. Solubility of aspirin in supercritical carbon dioxide with and without acetone. *J. Chem. Eng. Data* **49**, 1323–1327. <https://doi.org/10.1021/jc0499465> (2004).
12. Hosseini, M. H., Alizadeh, N. & Khanchi, A. R. Effect of menthol as solid cosolvent on the solubility enhancement of clozapine and lamorgine in supercritical CO₂. *J. Supercrit. Fluids* **55**, 14–22. <https://doi.org/10.1016/j.supflu.2010.09.002> (2010).
13. Sodeifian, G. & Sajadian, S. A. Measuring and Modeling the Solubility of Pharmaceutical Substances for the Production of Nanoparticles Using Supercritical Fluid and Ultrasound Technology. *PhD thesis*, 211 (2018).
14. Sodeifian, G., Razmimanesh, F. & Sajadian, S. A. Solubility measurement of a chemotherapeutic agent (Imatinib mesylate) in supercritical carbon dioxide: Assessment of new empirical model. *J. Supercrit. Fluids* **146**, 89–99. <https://doi.org/10.1016/j.supflu.2019.01.006> (2019).
15. Sodeifian, G., Ardestani, N. S., Sajadian, S. A. & Panah, H. S. Experimental measurements and thermodynamic modeling of Coumarin-7 solid solubility in supercritical carbon dioxide: Production of nanoparticles via RESS method. *Fluid Phase Equilib.* **483**, 122–143. <https://doi.org/10.1016/j.fluid.2018.11.006> (2019).
16. Pitchaiah, K. C. *et al.* Experimental measurements and correlation of the solubility of N, N-dialkylamides in supercritical carbon dioxide. *J. Supercrit. Fluids* **143**, 162–170. <https://doi.org/10.1016/j.supflu.2018.08.007> (2019).
17. Sodeifian, G., Ardestani, N. S. & Sajadian, S. A. Solubility measurement of a pigment (Phthalocyanine green) in supercritical carbon dioxide: Experimental correlations and thermodynamic modeling. *Fluid Phase Equilib.* **494**, 61–73. <https://doi.org/10.1016/j.fluid.2019.04.024> (2019).
18. Sodeifian, G., Saadati Ardestani, N., Sajadian, S. A. & Soltani Panah, H. Experimental measurements and thermodynamic modeling of Coumarin-7 solid solubility in supercritical carbon dioxide: Production of nanoparticles via RESS method. *Fluid Phase Equilib.* **483**, 122–143. <https://doi.org/10.1016/j.fluid.2018.11.006> (2019).
19. Sodeifian, G., Draksheshpoor, R. & Sajadian, S. A. Experimental study and thermodynamic modeling of Esomeprazole (proton-pump inhibitor drug for stomach acid reduction) solubility in supercritical carbon dioxide. *J. Supercrit. Fluids* <https://doi.org/10.1016/j.supflu.2019.104606> (2019).
20. Sodeifian, G., Hazaveie, S. M., Sajadian, S. A. & Saadati Ardestani, N. Determination of the solubility of the repaglinide drug in supercritical carbon dioxide: Experimental data and thermodynamic modeling. *J. Chem. Eng. Data* **64**, 5338–5348. <https://doi.org/10.1021/acs.jced.9b00550> (2019).
21. Reddy, S. N. & Madras, G. Measurement and correlation of quaternary solubilities of dihydroxybenzene isomers in supercritical carbon dioxide. *J. Supercrit. Fluids* **73**, 63–69. <https://doi.org/10.1016/j.supflu.2012.11.003> (2013).
22. Shamsipur, M., Karami, A. R., Yamini, Y. & Sharghi, H. Solubilities of some 1-hydroxy-9, 10-anthraquinone derivatives in supercritical carbon dioxide. *J. Supercrit. Fluids* **32**, 47–53. <https://doi.org/10.1016/j.supflu.2004.01.006> (2004).
23. Sodeifian, G., Sajadian, S. A. & Ardestani, N. S. Optimization of essential oil extraction from *Launaea acanthodes* Boiss: Utilization of supercritical carbon dioxide and cosolvent. *J. Supercrit. Fluids* **116**, 46–56. <https://doi.org/10.1016/j.supflu.2016.05.015> (2016).
24. Sodeifian, G., Sajadian, S. A. & Ardestani, N. S. Experimental optimization and mathematical modeling of the supercritical fluid extraction of essential oil from *Eryngium billardieri*: Application of simulated annealing (SA) algorithm. *J. Supercrit. Fluids* **127**, 146–157. <https://doi.org/10.1016/j.supflu.2017.04.007> (2017).
25. Sodeifian, G. & Sajadian, S. A. Investigation of essential oil extraction and antioxidant activity of *Echinophora platyloba* DC. using supercritical carbon dioxide. *J. Supercrit. Fluids* **121**, 52–62. <https://doi.org/10.1016/j.supflu.2016.11.014> (2017).
26. Sodeifian, G., Sajadian, S. A. & Daneshyan, S. Preparation of Aprepitant nanoparticles (efficient drug for coping with the effects of cancer treatment) by rapid expansion of supercritical solution with solid cosolvent (RESS-SC). *J. Supercrit. Fluids* **140**, 72–84. <https://doi.org/10.1016/j.supflu.2018.06.009> (2018).
27. Sodeifian, G., Sajadian, S. A., Razmimanesh, F. & Ardestani, N. S. A comprehensive comparison among four different approaches for predicting the solubility of pharmaceutical solid compounds in supercritical carbon dioxide. *Korean J. Chem. Eng.* **35**, 2097–2116. <https://doi.org/10.1007/s11814-018-0125-6> (2018).
28. Chrastil, J. Solubility of solids and liquids in supercritical gases. *J. Phys. Chem.* **86**, 3016–3021. <https://doi.org/10.1021/j100212a041> (1982).
29. Kumar, S. K. & Johnston, K. P. Modelling the solubility of solids in supercritical fluids with density as the independent variable. *J. Supercrit. Fluids* **1**, 15–22. [https://doi.org/10.1016/0896-8446\(88\)90005-8](https://doi.org/10.1016/0896-8446(88)90005-8) (1988).
30. Del Valle, J. M. & Aguilera, J. M. An improved equation for predicting the solubility of vegetable oils in supercritical carbon dioxide. *Ind. Eng. Chem. Res.* **27**, 1551–1553. <https://doi.org/10.1021/ie00080a036> (1988).
31. Gordillo, M., Blanco, M., Molero, A. & De La Ossa, E. M. Solubility of the antibiotic Penicillin G in supercritical carbon dioxide. *J. Supercrit. Fluids* **15**, 183–190. [https://doi.org/10.1016/S0896-8446\(99\)00008-X](https://doi.org/10.1016/S0896-8446(99)00008-X) (1999).
32. Mendez-Santiago, J. & Teja, A. S. Solubility of solids in supercritical fluids: Consistency of data and a new model for cosolvent systems. *Ind. Eng. Chem. Res.* **39**, 4767–4771. <https://doi.org/10.1021/ie000339u> (2000).
33. Jouyban, A., Chan, H.-K. & Foster, N. R. Mathematical representation of solute solubility in supercritical carbon dioxide using empirical expressions. *J. Supercrit. Fluids* **24**, 19–35. [https://doi.org/10.1016/S0896-8446\(02\)00015-3](https://doi.org/10.1016/S0896-8446(02)00015-3) (2002).
34. Sparks, D. L., Hernandez, R. & Estévez, L. A. Evaluation of density-based models for the solubility of solids in supercritical carbon dioxide and formulation of a new model. *Chem. Eng. Sci.* **63**, 4292–4301. <https://doi.org/10.1016/j.ces.2008.05.031> (2008).
35. Chapman, W. G., Gubbins, K. E., Jackson, G. & Radosz, M. SAFT: Equation-of-state solution model for associating fluids. *Fluid Phase Equilib.* **52**, 31–38. [https://doi.org/10.1016/0378-3812\(89\)80308-5](https://doi.org/10.1016/0378-3812(89)80308-5) (1989).
36. Economou, I. G., Gregg, C. J. & Radosz, M. Solubilities of solid polynuclear aromatics (PNA's) in supercritical ethylene and ethane from statistical associating fluid theory (SAFT): Toward separating PNA's by size and structure. *Ind. Eng. Chem. Res.* **31**, 2620–2624. <https://doi.org/10.1021/ie00011a028> (1992).
37. McCabe, C. & Jackson, G. SAFT-VR modelling of the phase equilibrium of long-chain n-alkanes. *Phys. Chem. Chem. Phys.* **1**, 2057–2064. <https://doi.org/10.1039/A808085B> (1999).

38. Gross, J. & Sadowski, G. Perturbed-chain SAFT: An equation of state based on a perturbation theory for chain molecules. *Ind. Eng. Chem. Res.* **40**, 1244–1260. <https://doi.org/10.1021/ie0003887> (2001).
39. Hosseini Anvari, M. & Pazuki, G. A study on the predictive capability of the SAFT-VR equation of state for solubility of solids in supercritical CO₂. *J. Supercrit. Fluids* **90**, 73–83. <https://doi.org/10.1016/j.supflu.2014.03.005> (2014).
40. Peng, D.-Y. & Robinson, D. B. A new two-constant equation of state. *Ind. Eng. Chem. Fundam.* **15**, 59–64. <https://doi.org/10.1021/i160057a011> (1976).
41. Bian, X.-Q., Zhang, Q., Du, Z.-M., Chen, J. & Jaubert, J.-N. A five-parameter empirical model for correlating the solubility of solid compounds in supercritical carbon dioxide. *Fluid Phase Equilib.* **411**, 74–80. <https://doi.org/10.1016/j.fluid.2015.12.017> (2016).
42. Sodeifian, G., Sajadian, S. A. & Derakhsheshpour, R. Experimental measurement and thermodynamic modeling of Lansoprazole solubility in supercritical carbon dioxide: Application of SAFT-VR EoS. *Fluid Phase Equilib.* **507**, 112422. <https://doi.org/10.1016/j.fluid.2019.112422> (2020).
43. Sodeifian, G., Razmimanesh, F., Sajadian, S. A. & Panah, H. S. Solubility measurement of an antihistamine drug (loratadine) in supercritical carbon dioxide: Assessment of qCPA and PCP-SAFT equations of state. *Fluid Phase Equilib.* **472**, 147–159. <https://doi.org/10.1016/j.fluid.2018.05.018> (2018).
44. Cabral, V., Santos, W., Muniz, E., Rubira, A. & Cardozo-Filho, L. Correlation of dye solubility in supercritical carbon dioxide. *J. Supercrit. fluids* **40**, 163–169 (2007).
45. Bian, X.-Q., Zhang, Q., Zhang, L. & Chen, J. A grey wolf optimizer-based support vector machine for the solubility of aromatic compounds in supercritical carbon dioxide. *Chem. Eng. Res. Des.* **123**, 284–294. <https://doi.org/10.1016/j.cherd.2017.05.008> (2017).
46. Jouyban, A., Khoubnasabjafari, M. & Chan, H.-K. Modeling the entrainer effects on solubility of solutes in supercritical carbon dioxide. *Chem. Pharm. Bull.* **53**, 290–295. <https://doi.org/10.1248/cpb.53.290> (2005).
47. Keshmiri, K., Vatanara, A. & Yamini, Y. Development and evaluation of a new semi-empirical model for correlation of drug solubility in supercritical CO₂. *Fluid Phase Equilib.* **363**, 18–26. <https://doi.org/10.1016/j.fluid.2013.11.013> (2014).
48. Garlapati, C. & Madras, G. New empirical expressions to correlate solubilities of solids in supercritical carbon dioxide. *Thermochim. Acta* **500**, 123–127. <https://doi.org/10.1016/j.tca.2009.12.004> (2010).
49. Soltani, S. & Mazloumi, S. H. A new empirical model to correlate solute solubility in supercritical carbon dioxide in presence of co-solvent. *Chem. Eng. Res. Des.* **125**, 79–87. <https://doi.org/10.1016/j.cherd.2017.07.006> (2017).
50. Reddy, T. A. & Garlapati, C. Dimensionless empirical model to correlate pharmaceutical compound solubility in supercritical carbon dioxide. *Chem. Eng. Technol.* **42**, 2621–2630. <https://doi.org/10.1002/ceat.201900283> (2019).
51. Bartle, K. D., Clifford, A. A., Jafar, S. A. & Shilstone, G. F. Solubilities of solids and liquids of low volatility in supercritical carbon dioxide. *J. Phys. Chem. Ref. Data* **20**, 713–756. <https://doi.org/10.1063/1.555893> (1991).
52. González, J. C., Vieytes, M. R., Botana, A. M., Vieites, J. M. & Botana, L. M. Modified mass action law-based model to correlate the solubility of solids and liquids in entrained supercritical carbon dioxide. *J. Chromatogr. A* **910**, 119–125. [https://doi.org/10.1016/S0021-9673\(00\)01120-1](https://doi.org/10.1016/S0021-9673(00)01120-1) (2001).
53. Méndez-Santiago, J. & Teja, A. S. The solubility of solids in supercritical fluids. *Fluid Phase Equilib.* **158**, 501–510. [https://doi.org/10.1016/S0378-3812\(99\)00154-5](https://doi.org/10.1016/S0378-3812(99)00154-5) (1999).
54. Sodeifian, G., Nasri, L., Razmimanesh, F. & Abadian, M. Measuring and modeling the solubility of an antihypertensive drug (losartan potassium, Cozaar) in supercritical carbon dioxide. *J. Mol. Liquids* <https://doi.org/10.1016/j.molliq.2021.115745> (2021).
55. Sodeifian, G., Garlapati, C., Razmimanesh, F. & Sodeifian, F. Solubility of amlodipine besylate (calcium channel blocker drug) in supercritical carbon dioxide: Measurement and correlations. *J. Chem. Eng. Data* **66**, 1119–1131. <https://doi.org/10.1021/acs.jced.0c00913> (2021).
56. Sodeifian, G., Razmimanesh, F., Ardestani, N. S. & Sajadian, S. A. Experimental data and thermodynamic modeling of solubility of Azathioprine, as an immunosuppressive and anti-cancer drug, in supercritical carbon dioxide. *J. Mol. Liq.* **299**, 112179. <https://doi.org/10.1016/j.molliq.2019.112179> (2020).
57. Sodeifian, G., Alwi, R. S., Razmimanesh, F. & Tamura, K. Solubility of quetiapine hemifumarate (antipsychotic drug) in supercritical carbon dioxide: Experimental, modeling and hansen solubility parameter application. *Fluid Phase Equilib.* <https://doi.org/10.1016/j.fluid.2021.113003> (2021).
58. Sodeifian, G. & Sajadian, S. A. Experimental measurement of solubilities of sertraline hydrochloride in supercritical carbon dioxide with/without menthol: Data correlation. *J. Supercrit. Fluids* **149**, 79–87. <https://doi.org/10.1016/j.supflu.2019.03.020> (2019).
59. Span, R. & Wagner, W. A new equation of state for carbon dioxide covering the fluid region from the triple-point temperature to 1100 K at pressures up to 800 MPa. *J. Phys. Chem. Ref. Data* **25**, 1509–1596. <https://doi.org/10.1063/1.555991> (1996).
60. Sodeifian, G., Sajadian, S. A. & Ardestani, N. S. Determination of solubility of Aprepitant (an antiemetic drug for chemotherapy) in supercritical carbon dioxide: Empirical and thermodynamic models. *J. Supercrit. Fluids* **128**, 102–111. <https://doi.org/10.1016/j.supflu.2017.05.019> (2017).
61. Wang, X. *et al.* Characterization and stability of tanshinone IIA solid dispersions with hydroxyapatite. *Materials* **6**, 805–816 (2013).
62. Sodeifian, G., Sajadian, S. A. & Razmimanesh, F. Solubility of an antiarrhythmic drug (amiodarone hydrochloride) in supercritical carbon dioxide: Experimental and modeling. *Fluid Phase Equilib.* **450**, 149–159. <https://doi.org/10.1016/j.fluid.2017.07.015> (2017).
63. Perrotin-Brunel, H. *et al.* Solubility of Δ 9-tetrahydrocannabinol in supercritical carbon dioxide: Experiments and modeling. *J. Supercrit. Fluids* **52**, 6–10. <https://doi.org/10.1016/j.supflu.2009.12.001> (2010).
64. Thakur, R. & Gupta, R. B. Rapid expansion of supercritical solution with solid cosolvent (RESS-SC) process: Formation of griseofulvin nanoparticles. *Ind. Eng. Chem. Res.* **44**, 7380–7387. <https://doi.org/10.1021/ie050417j> (2005).
65. Sabet, J. K., Ghotbi, C., Dorkoosh, F. & Striolo, A. Solubilities of acetaminophen in supercritical carbon dioxide with and without menthol cosolvent: Measurement and correlation. *Sci. Iran.* **19**, 619–625 (2012).
66. Thakur, R. & Gupta, R. B. Formation of phenytoin nanoparticles using rapid expansion of supercritical solution with solid cosolvent (RESS-SC) process. *Int. J. Pharm.* **308**, 190–199. <https://doi.org/10.1016/j.ijpharm.2005.11.005> (2006).
67. Bitencourt, R. G., Palma, A. M., Coutinho, J. A., Cabral, F. A. & Meirelles, A. J. Prediction of solid solute solubility in supercritical CO₂ with cosolvents using the CPA EoS. *Fluid Phase Equilib.* **482**, 1–10. <https://doi.org/10.1016/j.fluid.2018.10.020> (2019).
68. Jouyban, A. *et al.* Solubility prediction in supercritical CO₂ using minimum number of experiments. *J. Pharm. Sci.* **91**, 1287–1295. <https://doi.org/10.1002/jps.10127> (2002).
69. Montgomery, D. C. *Design and analysis of experiments* (John Wiley & sons, 2017).

Acknowledgements

Hereby, the researchers thank the great financial supports supplied by the research deputy of University of Kashan for supporting the present applied, beneficial, and worthwhile plan (Grant # Pajoohaneh-1398/9). Moreover, the researchers appreciate the Arasto Pharmaceutical Company.

Author contributions

G.S.: Conceptualization, Methodology, Validation, Investigation, Supervision, Writing—review & editing. S.A.S.: Methodology, Investigation, Project administration. F.R.: Writing—original draft, Investigation, Resources. S.M.H.: Funding acquisition.

Competing interests

The authors declare no competing interests.

Additional information

Correspondence and requests for materials should be addressed to G.S.

Reprints and permissions information is available at www.nature.com/reprints.

Publisher's note Springer Nature remains neutral with regard to jurisdictional claims in published maps and institutional affiliations.



Open Access This article is licensed under a Creative Commons Attribution 4.0 International License, which permits use, sharing, adaptation, distribution and reproduction in any medium or format, as long as you give appropriate credit to the original author(s) and the source, provide a link to the Creative Commons licence, and indicate if changes were made. The images or other third party material in this article are included in the article's Creative Commons licence, unless indicated otherwise in a credit line to the material. If material is not included in the article's Creative Commons licence and your intended use is not permitted by statutory regulation or exceeds the permitted use, you will need to obtain permission directly from the copyright holder. To view a copy of this licence, visit <http://creativecommons.org/licenses/by/4.0/>.

© The Author(s) 2021